Cellulose (2017) 24:2861–2875
DOI 10.1007/s10570-017-1316-8

ORIGINAL PAPER

Cellulose–halloysite nanotube composite hydrogels for curcumin delivery

Biao Huang · Mingxian Liu · Changren Zhou

Received: 24 January 2017 / Accepted: 27 April 2017 / Published online: 9 May 2017

Abstract Halloysite nanotubes (HNTs) were added to cellulose NaOH/urea solution to prepare composite hydrogels using epichlorhydrine crosslinking at an elevated temperature. The shear viscosity, mechanical properties, microstructure, swelling properties, cytocompatibility, and drug delivery behavior of the cellulose/HNT composite hydrogels were investigated. The viscosity of the composite solution increases with the addition of HNT. The compressive mechanical properties of composite hydrogels are significantly improved compared with pure cellulose hydrogel. The compressive strength of the composite hydrogels with 66.7% HNTs is 128 kPa, while that of pure cellulose hydrogel is only 29.8 kPa in compressive strength. Rheological measurement suggests the resistance to deformation is improved for composite hydrogels. X-ray diffraction and Fourier transform infrared spectroscopy show that the crystal structure and chemical structure of HNT are not changed in the composite hydrogels. Hydrogen bonding interactions between HNT and cellulose exist in the composites. A porous structure of the composite hydrogels with pore size of 200–400 μm was found by scanning electron microscopy. The addition of HNT leads to decreased swelling ratios in NaCl solution and pure water for the composite hydrogels. Cytotoxicity assays show that the cellulose/HNT composite hydrogels have a good biocompatibility with MC3T3-E1 cells and MCF-7 cells. Curcumin is further loaded into the composite hydrogel via physical adsorption. The curcumin-loaded composite hydrogels show a strong inhibition effect on the cancer cells. All the results illustrate that the cellulose/HNT composite hydrogels have promising applications such as anticancer drug delivery systems and anti-inflammatory wound dressings.

Keywords Halloysite · Cellulose · Hydrogels · Biocompatibility · Drug delivery

B. Huang · M. Liu (✉) · C. Zhou
Department of Materials Science and Engineering, Jinan University, Guangzhou 510632, China
e-mail: liumx@jnu.edu.cn

Introduction

In the last decade, natural occurred biopolymers with a well-defined structure have gained more and more attention due to their many advantages such as low toxicity, biocompatibility, degradation, and good fiber-forming, film-forming abilities. Among them, cellulose is the most abundant linear polysaccharide polymer on the earth, which represents an important material for producing biocompatible products (Eichhorn et al. 2010; Klemm et al. 2005). Cellulose has been widely applied as biodegradable plastics, fibers and clothes, drug delivery carriers, bone repairing materials, and foods (De Oliveira Barud et al. 2016; Wan et al. 2017). However, raw cellulose is hard to process into materials due to the strong intra- or inter-

molecular hydrogen bonds. Cellulose cannot be dissolved in water and general organic solvents. It is also hard to process in melt because of the closed melting temperature and degradation temperature. Zhang et al. invented a new high-efficient dissolving method for cellulose using alkali/urea systems, which promotes the practical applications of cellulose-related materials in various areas (Cai and Zhang 2005; Cavallaro et al. 2014; French 2014). Transparent cellulose alkali/urea solution can be transferred into films, hydrogels, fibers, and porous scaffolds, which have shown promising applications in biomedical areas (Meibom et al. 2004; Pandey et al. 2017; Price et al. 2001). However, the weak mechanical strength, lack of interactions with cells, and poor drug loading ability of cellulose limit its application.

Incorporation of nanoparticles to the cellulose is an efficient solution to address these shortcomings. The many hydroxyl groups in the cellulose chains can be used to bond the nanoparticles via hydrogen bonding, which always leads to significantly improved mechanical properties and new functions (Cai et al. 2012; Liu et al. 2016a, 2016c; Miao and Hamad 2013; Yu et al. 2013). Many types of nanoparticles, including organic, metal, and inorganics, have been used to compound with cellulose to obtain high performance or functional composites. For example, cellulose nanocrystals exhibited significant reinforcement characteristics for the storage modulus in cellulose acetate butyrate matrixes. Cellulose–silver nanocomposites fabricated by reducing silver nitrate in ethylene glycol method possess a high antimicrobial activity against *Escherichia coli* and *Staphylococcus aureus* (Li et al. 2011). Composite film composed of gold nanorods and cellulose acetate can be used as biosensors of glucose (Ren et al. 2009). Metallic nano-oxides such as zinc oxide were also added to the cellulose to increase the antibacterial activity of the material for wound dressing applications (Maneerung et al. 2008). Inorganic nanoparticles are incorporated into cellulose to improve the strength and toughness of the material. Cellulose–silica composite aerogels prepared via solution mixing exhibited a reinforcing effect (Demilecamps et al. 2014). Good dispersion and alignment of multiwalled carbon nanotubes (MWCNTs) in cellulose was also achieved by dissolution in an ionic liquid and subsequent grinding and spinning. The regenerated-cellulose/MWCNT composite fibers exhibited improved mechanical properties and thermal stability (Zhang et al. 2007). Regenerated cellulose/graphene composite films prepared by dispersing graphene into cellulose solutions in DMAC/LiCl also showed improved thermal stability, electrical conductivity, and mechanical properties of the composite materials (Zhang et al. 2012). Although these nanoparticles can be successfully applied for preparation of cellulose composites, novel nanoreinforcements with good biocompatibility and low price still are needed for practical applications in biomedical areas.

Naturally occurred halloysite nanotubes (HNTs) possess unique empty lumen tubular morphology in nanoscales with high aspect ratio, high strength, and a similar chemical formula with kaolinite ($Al_2Si_2O_5(OH)_4{\cdot}nH_2O$), which show a promising application in polymer composites. The advantages of HNT used for biomedical composites include high adsorption ability, low toxicity, good biocompatibility, and being inexpensive (Liu et al. 2007, 2014a, b, 2013a, 2010). For example, it can be used as drug delivery carriers for curcumin, doxorubicin (DOX), DNA, protein, and antibacterial agents (Abdullayev et al. 2012; Yang et al. 2016). HNTs can protect the drug from enzyme degradation and can enter the cell for delivery of the drugs. HNTs have diameters of 20–50 nm and lengths of 200–1000 nm, which give a high aspect ratio of 10–100. So, HNTs can be incorporated into polymer porous scaffolds for high-performance tissue engineering scaffolds and wound dressing materials (Liu et al. 2013a, 2014b, Pandey et al. 2017). Patterned HNT nanosurfaces can also been used to capture circulating tumor cells from peripheral blood, which shows promising application in cancer early diagnose (Ariga et al. 2011; Liu et al. 2016b; Lvov et al. 2008; Yang et al. 2016). Recently, HNTs were added into cellulose to improve the mechanical properties of the cellulose composite hydrogel by dissolving the cellulose in ionic liquid (Hanid et al. 2014; Soheilmoghaddam et al. 2013). However, the low dissolution efficient and the high cost of ionic liquids limit their practical applications.

In this work, cellulose/HNT composite hydrogels were prepared by dispersing HNT powder into cellulose alkali/urea solutions and then forming hydrogels using epichlorhydrine crosslinking at elevated temperatures. The physical properties, chemical structure, and cytocompatibility, of the composite hydrogels are characterized. HNTs can significantly improve the

mechanical properties of cellulose composites and show good cytocompatibility. Furthermore, curcumin was used as a model drug to study the drug-release properties of the composite hydrogels (Cavallaro et al. 2014; Lvov et al. 2016; Price et al. 2001). The curcumin-loaded composite hydrogels show a strong inhibition effect on the cancer cells. It is expected that the biocompatible composite hydrogel with high strength can be used in an anticancer drug delivery system and anti-inflammatory wound dressings.

Experimental

Materials

High-purity halloysite nanotubes (HNTs) were purchased from Guangzhou runwo materials technology Co., Ltd, China. The cellulose powder with particle size of 25 μm and other reagents were purchased from Aladdin (Shanghai, China). Ultrapure water was used from a Milli-Q water system (resistivity >18 MΩ cm^{-1}). Acridine orange-ethidium bromide (AO-EB), a Cell Counting Kit-8 (CCK-8), and Fluorescein isothiocyanate isomer I (FITC) were purchased from Nanjing Keygen Biotech Co., Ltd.

Preparation of cellulose/HNT composite hydrogels

Cellulose was dissolved in alkali/urea solutions according to the references (Cai and Zhang 2005). Briefly, cellulose powder was dispersed in 4 wt% LiOH and 7 wt% urea solution via mechanical stirring. Subsequently, the dispersion was frozen at −20 °C overnight. Then the dispersion was thawed out and stirred at 5 °C to form a transparent cellulose solution with 4 wt% cellulose concentrations. The clear and colorless cellulose solution was centrifuged at 5 °C at 7000 rpm for 15 min to remove the air bubbles. Cellulose/HNT composite hydrogels were prepared by adding 1, 2, 4, and 8 g HNT powder into a 100 mL cellulose solution by ultrasonic treatment (50 W × 10 min) and mechanically stirring (1000 rpm × 30 min) to obtain a series of cellulose/HNT composite solutions (the weight ratio of HNT and cellulose was 4:1, 2:1, 1:1, and 1:2). Then 3 mL epichlorhydrine (ECH) was added into the above cellulose/HNT composite solution and stirred at room temperature for 30 min. The resultant solution was cast on the test tube with inner diameter ∼11 mm and formed a hydrogel at 60 °C for 1 h. Subsequently the hydrogels were taken out from the mold and thoroughly washed with deionized water to remove remaining alkali/urea. The cellulose hydrogel without addition of HNT was coded as Ce. The number in the code of the composite hydrogel of Ce4N1, Ce2N1, Ce1N1, and Ce1N2 represented the weight ratio of cellulose and HNT. All the hydrogels were stored in deionized water at 4 °C before characterization.

Characterization

Firstly, 0.05 wt% of HNT aqueous dispersions was dropped in a carbon membrane supported copper mesh and dried naturally. The samples were then observed on Philips Tecnai-10 transmission electron microscopy (TEM) at an accelerating voltage of 100 kV. Scanning electron microscopy (SEM) of HNT was observed by dropping 0.05 wt% HNT aqueous dispersions in glass substrates and drying naturally. Before observation, the sample was sputtered with a layer of gold. The SEM images were obtained with a Zeiss Ultra 55 SEM machine at 5 kV.

The dynamic viscosity of the cellulose and cellulose/HNT mixture solutions was measured by a rotating rheometer (Kinexus pro+, Malvern Instruments, Malvern, UK) at 25 °C with the shear rate of 1–100 s^{-1}. A SHIMADZU AG-1 machine was used to test the compressive mechanical property of the hydrogels under 25 °C at a speed of 2 mm/min. The storage modulus of the hydrogels also was analyzed in room temperature with strains sweep (0.1–100%) and frequency scanning (0.1–100 Hz) by a rotating rheometer (Kinexus pro^{+}, Malvern Instruments, Malvern, UK). The samples with a diameter of 15 mm were cut into slices of ∼0.1 cm thickness. The strain sweep was carried out at a fixed frequency of 1 Hz, and the frequency sweep was carried out at the fixed strain of 0.5%. The pore structure of the hydrogels was characterized by scanning electron microscopy (SEM) (S-4800 FE, Hitachi) at a voltage of 2 kV. The wet hydrogels were freeze–dried, sectioned, and sputtered with gold before observation. The hydrogels were then stained by FITC, freeze–dried, and observed using fluorescent microscope (XDY-2, Yuexian optical instruments, Guangzhou, China). X-Ray Diffraction (XRD) profiles for samples were obtained using an X-ray diffractometer (MiniFlex-600, Rigaku

Corporation, Japan) at 25 °C. The scanning angle was from 5° to 80° with a scanning speed of 10°/min at 40 kV voltages and 15 mA current. The milled powder of freeze-dried hydrogel samples were analyzed in FTIR spectrometer (VERTEX 70, Bruker) from 400 to 4000 cm^{-1}. The swelling behavior of hydrogels was determined in the water and a 0.1 M sodium chloride solution. The equilibrium swelling ratios (ESR) was determined as:

$$ESR = (W_s - W_d)/W_d$$

where, W_s was the weight the swollen hydrogels at 37 °C, and W_d was the weight of the oven-dried hydrogels.

Cytotoxicity

Mouse embryo osteoblast precursor cells (MC3T3-E1) and human breast adenocarcinoma cells (MCF-7) were cultured in Dulbecco's Modified Eagle's Medium (DMEM). Hydrogel films 1 mm thick were sterilized by autoclave sterilizers. After cultured for 48 and 72 h, the MC3T3-E1 cells on material were stained with AO/EB and then observed under a fluorescent microscope (XDY-2, Yuexian optical instruments, Guangzhou, China). The CCK-8 assay was used to investigate the cell activity in a Microplate System (Thermo, Multiskn MK3, Shanghai, China). Cells were seeded onto the material for 48 and 72 h, and then 10 μL of CCK-8 solution was added to each well and continuously incubated in the cell incubator for another 4 h. The OD value was read at wavelength 450 nm in 96-well plates.

Drug loading and release studies

The Ce and Ce2N1 hydrogels with thickness of 1 mm were vacuum-dried at 60 °C for 24 h to remove any residual moisture. Afterwards, the dried hydrogels was incubated in 10 mL (1 g/mL) of curcumin/ethanol solution for 48 h in the darkness. The determination of loading capacity and drug entrapment efficiency of hydrogels were based on a standard curve method using the formula.

$$\text{Loading capacity} = (W_{total} - W_{remain})/W_{sample} \times 100\%$$

$$\text{Entrapment efficiency} = (W_{total} - W_{remain})/W_{total} \times 100\%$$

where, W_{total}, W_{remain}, and W_{sample} represent the initial curcumin content, the amount of the remaining curcumin in the solution, and the total mass of hydrogel sample after drug-loading, respectively.

Drug loaded hydrogels were soaked in 50 mL pure ethanol medium in incubator shakers at 37 °C. A 0.5 mL solution was taken out for absorbance determination every 2 h, and 0.5 mL fresh ethanol solution was added to replenish the original solution. The amount of curcumin was assayed using an UV–visible spectrometer (UV-2550, Shimadzu Instrument Ltd., Suzhou, China) at 420 nm. The released amount was obtained by calculating the drug amount in an ethanol medium by comparing with the standard curve.

For in vitro cytotoxicity study, the hydrogels containing curcumin was taken out from ethanol solution and swollen in sterile water at 60 °C to remove excess ethanol. MC3T3-E1 cell and MCF-7 cells were seeded in hydrogels at approximately 50,000 cells/well and culture 48 and 72 h. Then the cells on the materials were stained with AO/EB and then observed under a fluorescent microscope. The cell viability was also assessed using the CCK-8 method as described above.

Results and discussion

Characterization of HNT and the cellulose/HNT composite solution

TEM and SEM images of the used HNTs are shown in Fig. 1. It can be seen that HNTs show tubular morphology with empty lumen. The length and diameter of HNT vary widely in size. The length ranges from 20 to 1500 nm, while the outer diameter ranges from 20 to 70 nm. The high aspect ratio of HNT is beneficial to improve the stability of the cellulose/HNT composite solutions and the mechanical properties of the composite hydrogels. HNT surface is negatively charged with zeta potential of −25.0 mV. Also, the cellulose carries a small negative charge due to the presence of some carboxylic acid groups from oxidation at the primary hydroxylic sites. So, HNTs were dispersed in cellulose solution by continuous ultrasonic treatment and mechanical stirring. The viscosity of polymer solution can be increased by the addition of HNT (Huang et al.

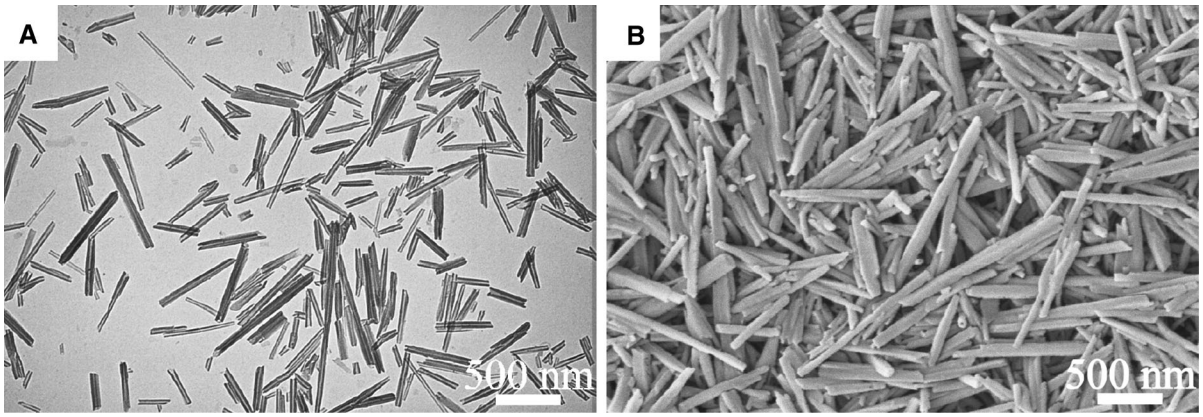

Fig. 1 TEM (**a**) and SEM (**b**) photographs of HNT

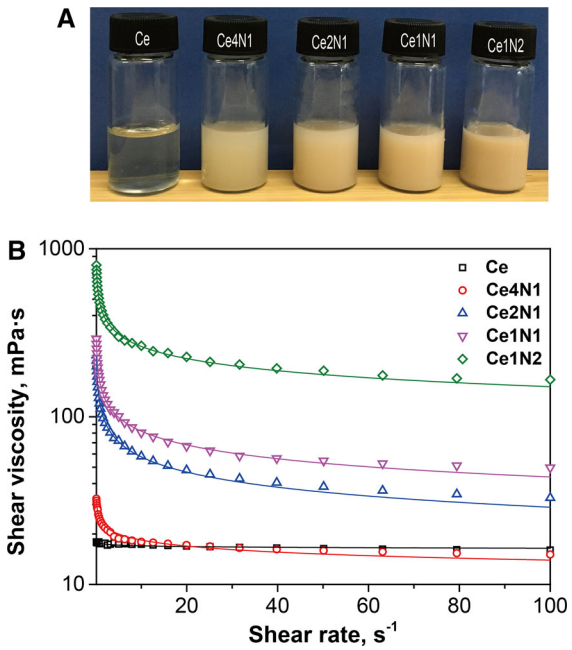

Fig. 2 **a** Photographs of cellulose and cellulose/HNT composite solution. **b** The shear viscosity curve of cellulose and cellulose/HNT composite solution

2017; Liu et al. 2013a). A similar trend was also found in the cellulose/HNT composite solution. As shown in Fig. 2a, the pure cellulose solution is a clear and transparent liquid with low viscosity. As the content of HNT increases, the solutions become turbid and opaque with increased viscosity. This is attributed to the thickening effect of HNT by the formed HNT network in the solution. The effect of HNT on the solution viscosity of cellulose is quantitatively compared in Fig. 2b. When the shear rate increases from 0.1 to 100 s^{-1}, the viscosity of the composites solution is higher than that of the cellulose solution. For example, the Ce1N2 solution shows 187.7 mPa s viscosity, which is only 16.7 mPa s for a cellulose solution at the shear rate of 40 s^{-1}. For the composite solution, the viscosity decreases with the increase of shear rate. For example, the viscosity of Ce1N2 solution decreases from 789.4 to 151.3 mPa s. This suggests that the composite solutions exhibit a shear-thinning effect. In contrast, the shear viscosity of pure cellulose solution is almost unchanged. No filler network is present in the pure cellulose solution, so the viscosity is not dependent on the shear rate. The viscosity significantly decreases with the increase of the shear rate in the composite solution, suggesting the formation of a HNT network in the cellulose matrix. The hydrogen bonding interactions between HNT and cellulose may also contribute to the increase in the viscosity, which will be shown in the following section.

Mechanical properties of cellulose/HNT composite hydrogels

Addition of nanoparticles with high aspect ratios always leads to the improvement of the mechanical properties. The effect of HNT content on the compressive properties of cellulose hydrogels was investigated. Figure 3A shows a series of photographs when putting pressure on Ce, Ce2N1, and Ce1N2 hydrogels with the same bulk size. Ce and Ce2N1 hydrogels are broken when the strain reaches 55%. However, the

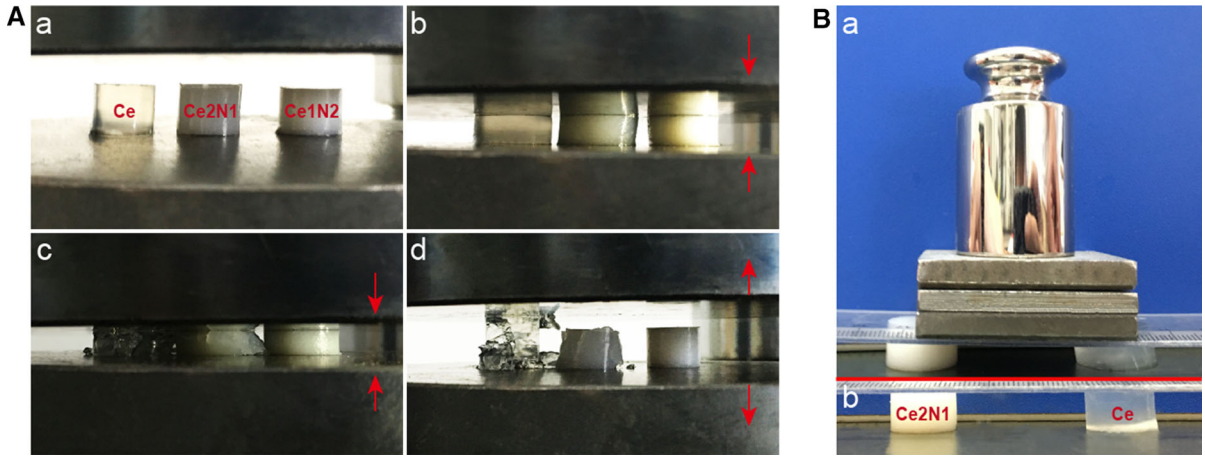

Fig. 3 **A** The compression behavior of the Ce, Ce2N1, and Ce1N2 before (*a*), during (*b*), and with 55% strain (*c*), recovery after compression (*d*). **B** load-bearing determination of Ce and Ce2N1 hydrogel with a weight of 270 g

Ce1N2 hydrogel can quickly recover their original shape without any rupture upon removing the load. Similarly, when Ce and Ce2N1 hydrogels are loaded (Fig. 3B) with a 270 g weight, the deformation of Ce hydrogels is significantly larger than that of Ce2N1. This suggests that the incorporation of HNT can greatly improve the strength and recovery of cellulose hydrogel.

Figure 4 shows the curves of compressive mechanical properties both in static and dynamic states of cellulose/HNT composite hydrogels. The mechanical properties of composite hydrogels are superior to pure Ce hydrogel in strength and strain at fracture (Table 1). When the HNT's content increases, the compressive strength of the composite hydrogels improves from 29.8 kPa of pure cellulose hydrogel to 128 kPa (Fig. 4a). From Fig. 4b, the compressive modulus of the composite hydrogel is also increased linearly with the content of HNT. Also, the Ce1N2 hydrogel exhibits the highest fracture strain in all the experimental groups. This suggests that HNTs have high reinforcing ability towards cellulose. The inset in Fig. 4a shows the appearance of the hydrogels. The pure cellulose hydrogel is totally transparent, while the composite hydrogels exhibit gradually opaque due to the presence of HNT. By touching them with finger, an obviously improved stiffness of composite hydrogels is found comparing with the pure cellulose hydrogel. Furthermore, composite hydrogels are more easily recoverable after stretching at 30, 40, and 50% strain than pure cellulose hydrogel under loading–unloading cycles (Fig. 4c, d). The Ce2N1 hydrogel nearly can recover its original shape after unloading for each cycle, while the Ce hydrogel is broken at the strain of 47%. This confirms the addition of HNT can improve both the strength and toughness of the cellulose hydrogels.

The strength and deformation restorability of the hydrogels were further investigated by rheology testing. When the frequency is increased from 0.1 to 100 Hz (Fig. 4e), the storage modulus (G') of composite hydrogels improves with HNT concentration especially at relatively low frequency (below 10 Hz). For example, the G' of Ce1N2 is 300 Pa at 1 Hz, which is three fold of that of pure cellulose hydrogel. The differences among the groups become negligible at high frequency, which is attributed to all the hydrogels exhibiting dramatically increased G'. The similar trend is also found in previous studies (Liu et al. 2012, 2015). Figure 4f further shows G' curves in a strain sweep of cellulose and cellulose/HNT hydrogels. Pure Ce hydrogel shows the lowest G' among all the samples in the entire determined strain region. All samples exhibit a G' platform at low strain and G' subsequently decrease with further increasing of strain. Ce1N2 hydrogel keeps the structural stability until 8% strain, while the G' of pure Ce hydrogel starts to decrease at a strain of 2%. The decrease in G' means a fracture of material or network deformation. These results demonstrate that the composite hydrogels have much higher mechanical

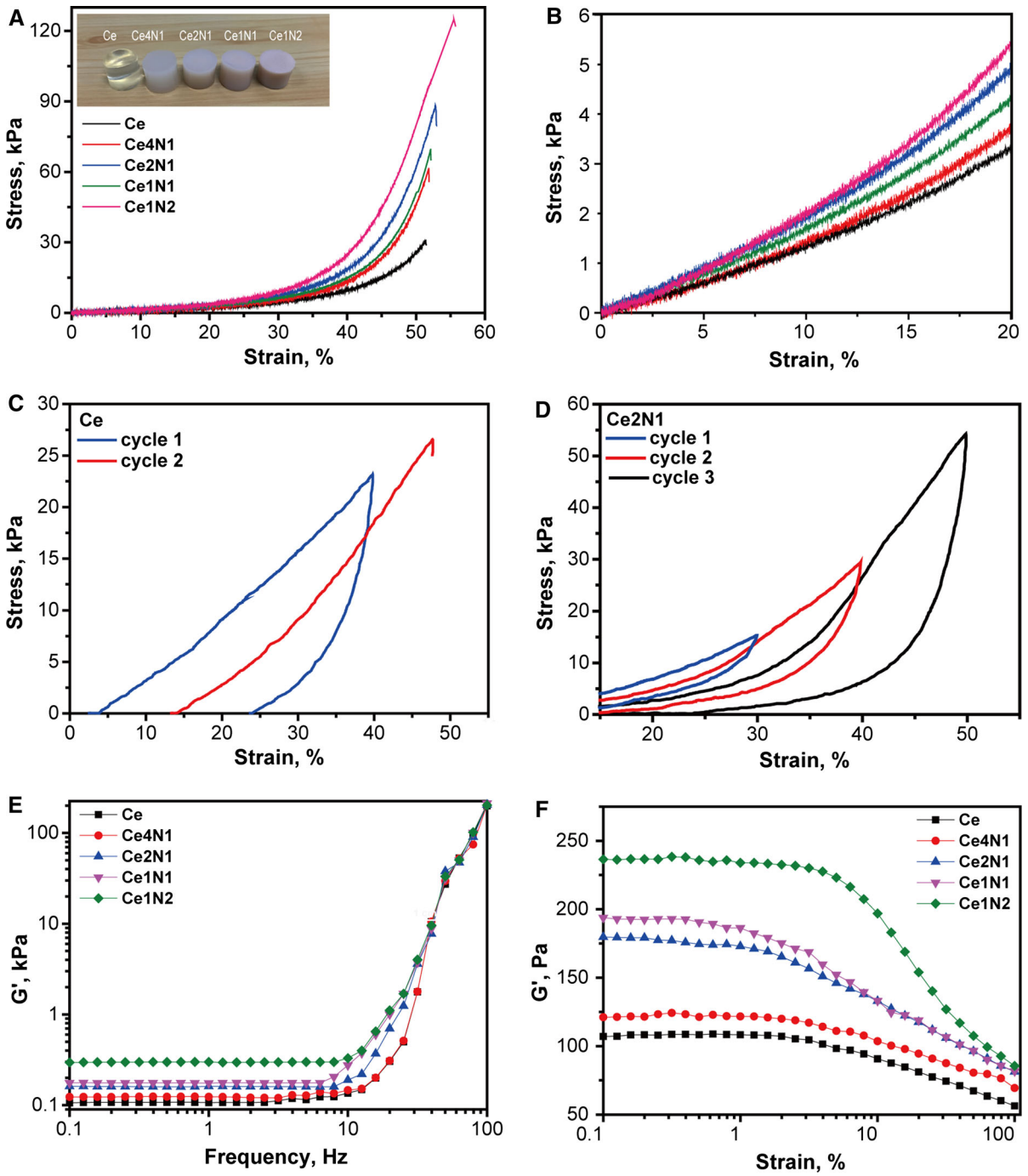

Fig. 4 Compressive curves of cellulose/HNT composite hydrogels (**a**) and enlarged curves of (**a**) in the strain range of 0–20% (**b**). Cyclic compression testing curve of Ce hydrogel (**c**) and Ce2N1 hydrogel (**d**). Storage modulus versus frequency (**e**) and strains (**f**) of Ce and Ce/HNT composite hydrogels

properties and flexibility than pure Ce hydrogel. Due to the interactions between HNT and cellulose, the HNTs in the hydrogel act as physical crosslinking points in the hydrogels which causes an appreciable change in the physical properties (Russo et al. 2007; Suzuki and Hanabusa 2010; Zhu et al. 2006).

Table 1 The mechanical properties of cellulose/HNT composite hydrogels

Hydrogel sample	Compressive strength (kPa)	Strain at break (%)	Storage modulus at frequency of 1 Hz and fixed strain of 0.5% (Pa)	Storage modulus at strain of 1% and fixed frequency of 1 Hz (Pa)
Ce	29.8	51.3	100.2	107.1
Ce4N1	59.8	51.7	125.3	120.0
Ce2N1	69.2	52.1	154.7	178.4
Ce1N1	87.3	52.8	179.6	194.1
Ce1N2	128	55.5	300.5	236.2

Structural characterization of cellulose/HNT composite hydrogels

The influence of HNT on the chemical structure and crystalline structure of cellulose were further investigated by FITR and XRD. As shown in Fig. 5a, the broad absorption bands of the cellulose and cellulose/HNT composite hydrogels at 3300–3400 cm^{-1} are assigned to stretching of hydroxyl groups. The absorption peaks of asymmetric and symmetric stretching vibration of CH_2 of cellulose is appeared at 2920 and 2869 cm^{-1}. HNTs show characteristic peaks at 3692 and 3621 cm^{-1} attributed to the stretching of inner-surface hydroxyl groups and inner hydroxyl groups, respectively (Yuan et al. 2008). The contents of the characteristic peaks at 3692 and 3621 cm^{-1} of HNT increase with the increasing in the HNT loading in the composite, which suggests the successfully blending of these two components. There is a down-shifting tendency of the absorption peaks of hydroxyl groups in the cellulose chains for cellulose/HNT composite hydrogels. The result indicates that the hydrogen bonds existed between cellulose and HNT. The hydrogen bond interactions in the components composites endow the composites with higher mechanical and thermal properties.

The XRD patterns for all the hydrogel samples are presented in Fig. 5b. The regenerated cellulose clearly exhibits a broad peak around 21° with full width at half maximum (FWHM) of ~9.8°, which suggests that the cellulose is amorphous (Ciolacu et al. 2011; French 2014). This is attributed to the alkali/urea aqueous solution breaking the crystalline structure of cellulose. The original HNT sample exhibited diffraction peaks in $2\theta = 11.7°, 20.1°, 24.7°$, and 35° assigned to (001), (020, 110), (002), (200, 130) plane, respectively (Abdullayev et al. 2012; Liu et al. 2013a; Pandey et al. 2017). No reflection peak near 10 Å can be

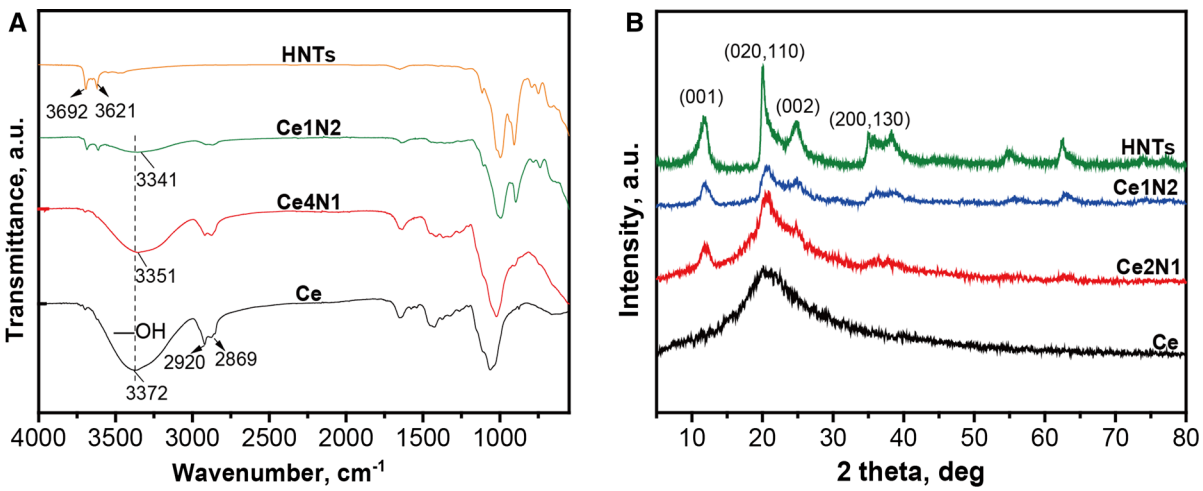

Fig. 5 FTIR spectra (**a**) and XRD patterns (**b**) of HNT, cellulose, and cellulose/HNT composites

observed in all the samples, suggesting the dehydrated state of HNT. It can be seen that the intensity of the HNT diffraction peak increases with the loading of HNT in the cellulose/HNT composites. The peak assigned to cellulose gradually decreases with the increase of HNT content, indicating strong interactions between cellulose and HNT.

Morphology and swelling studies of cellulose/HNT composite hydrogels

The pore structures of freeze-dried cellulose/HNT composite hydrogels were characterized by SEM images (Fig. 6a). It can be observed that the pore size decreases from ~400 to ~200 μm with the increase of HNT content. This is caused by the decreased water content in the same volume hydrogels. Water is a porogen in the present hydrogel system, and the addition of HNT into the composite hydrogels leads to the decrease in water content of the same volume hydrogels. As a result, the addition of HNT results in decreased pore size during the freeze-drying process (Huang et al. 2017). After carefully observing the SEM photographs, it can be found that the pore wall is smooth. However, the pore surfaces of the composite hydrogels are rougher with the increase in the concentration of HNT and a small amount of granular protrusion appears. This is due to presence of HNT and HNT aggregates in the composites. The suitable pore dimension with rough pore walls surfaces of the composites can provide high surface areas for cell attachments and drug loading because of the increased interfacial interactions. Figure 6b shows the fluorescent images of a cross-section of pure cellulose and cellulose/HNT composite hydrogels which are stained by FITC. It also can be seen almost the pores exhibit interconnected structures with pore diameter in the range from ~200 to ~400 μm. The thickness of the pore walls is in the range of ~20 to ~50 μm. A similar pore structure of HNT that incorporated polymer hydrogels has also been previously reported (Huang et al. 2017; Liu et al. 2013b).

The influence of HNT on the swelling ratios of the cellulose/HNT hydrogels were further evaluated in NaCl and water solution (Fig. 7). The Ce and cellulose/HNT hydrogels were firstly placed in a vacuum drying oven at 60 °C and dried for 24 h to obtain the dry gels. The volume of hydrogels was sharply shrunk after drying (Fig. 7A-a). Then the dry hydrogels were placed in a 0.1 M NaCl solution to reach swelling equilibrium (Fig. 7A-b). Figure 7B shows the curves of swelling ratio changes with the swelling time for the hydrogels. The composite hydrogels exhibit gradually decreased swelling ratios with the increase of HNT

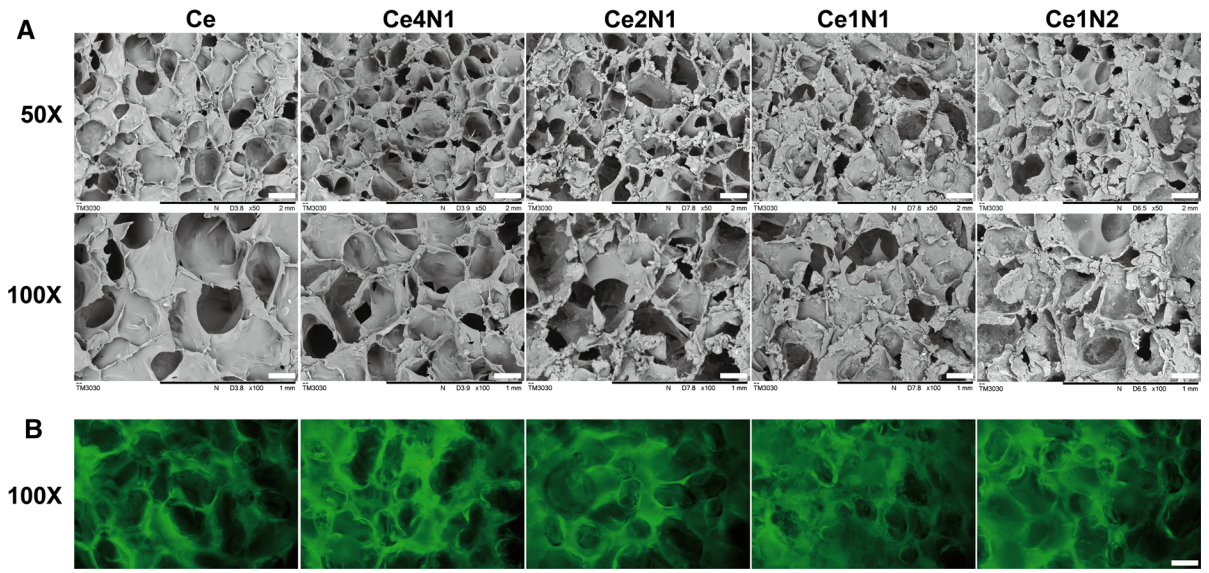

Fig. 6 **a** SEM images of a cross-section of pure cellulose and cellulose/HNT composite hydrogels. *Scale bar* ×50(400 μm), ×100 (200 μm). **b** Fluorescent images of a cross-section of pure cellulose and cellulose/HNT composite hydrogels stained by FITC. *Scale bar* 200 μm

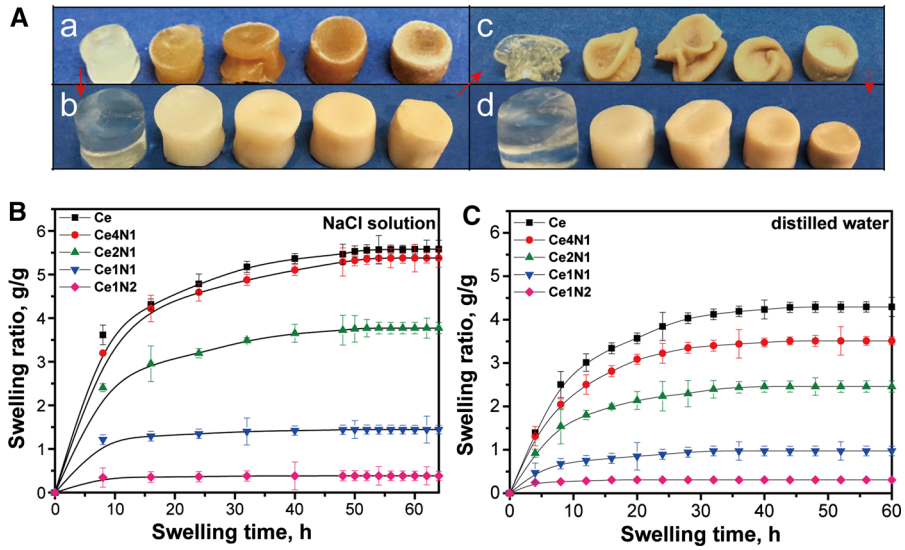

Fig. 7 **A** Photographs of hydrogels: (*a*) original hydrogels, (*b*) hydrogel swelled in NaCl solution, (*c*) the dried hydrogels (swollen hydrogels after vacuum-drying) and (*d*) hydrogel after re-swelling in distilled water. From left, Ce, Ce4N1, Ce2N1, Ce1N1, and Ce1N2. **B** Swelling kinetics of the Ce and cellulose/HNT composite hydrogels in a 0.1 M NaCl solution at 37 °C. **C** Re-swelling kinetics of the Ce and cellulose/HNT composite hydrogels in distilled water at 37 °C

content with the same swelling time. For instance, the Ce1N2 hydrogel shows an equilibrium swelling ratio of 0.5 which is much lower than that of Ce hydrogel (5.5). The decreased swelling ratio of composite hydrogels is caused by the decreased hydrophilic polymer content in the composites with the addition of HNT. From the shape of the change ratio in the Fig. 7A-b, a similar trend can also be found.

The re-swelling capabilities of the hydrogels were further evaluated by drying the swelled hydrogels and immersing them in distilled water. It also can be seen that the composite hydrogels exhibit gradually decreased swelling ratios with the increase of HNT content with the same swelling time. Compared with a NaCl solution, all hydrogels exhibit a decreased swelling ratio in water especially for the pure cellulose hydrogel and the composite hydrogels with low HNT loading. The swelling ratio of pure Ce hydrogel in water is 4.5 while it is 5.5 in a NaCl solution (Fig. 7C). There is a comparable swelling ratio for the Ce1N2 hydrogel, suggesting that the skeleton structure is almost unchanged for the swelling-reswelling process. So the swelling ratio of the cellulose hydrogel can be tailored by addition of a different content of HNT. The cellulose composite hydrogels with HNT can be used as biomaterial scaffolds because of their excellent structural stability in biological liquids.

Biocompatibility valuation of cellulose/HNT composite hydrogels

The cytotoxity of the composite hydrogels was assessed by the MC3T3-E1 and MCF-7 cell lines. Figure 8a shows fluorescent microscope images of the MC3T3-E1 cells cultured on different hydrogels. For AO/EB live/dead cell viability assays, live cells are identified on the basis of intracellular esterase activity (generating green fluorescence) and exclusion of the red dye. Dead cells are identified by the lack of esterase activity and non-intact plasma membrane which allows red dye staining. It can be seen that all the MC3T3-E1 cells on the hydrogel samples are in the form of long fusiform shapes. For all the groups, almost no dead cells can be found in the field of vision, indicating high cytocompatibility for the composite hydrogels. The number of living cells after 72 h are more than that of cells cultured for 48 h, which reveals that the good proliferation capacity of cells on the hydrogel surfaces. The addition of HNT has little effect on the cell viability from the morphological observations. Figure 8b, c show the CCK-8 cell viability of MC3T3-E1 and MCF-7 cells grown on the different hydrogels. Both kinds of cells show a high cell relative viability after 48 h. The composite hydrogels show much higher cell viability compared

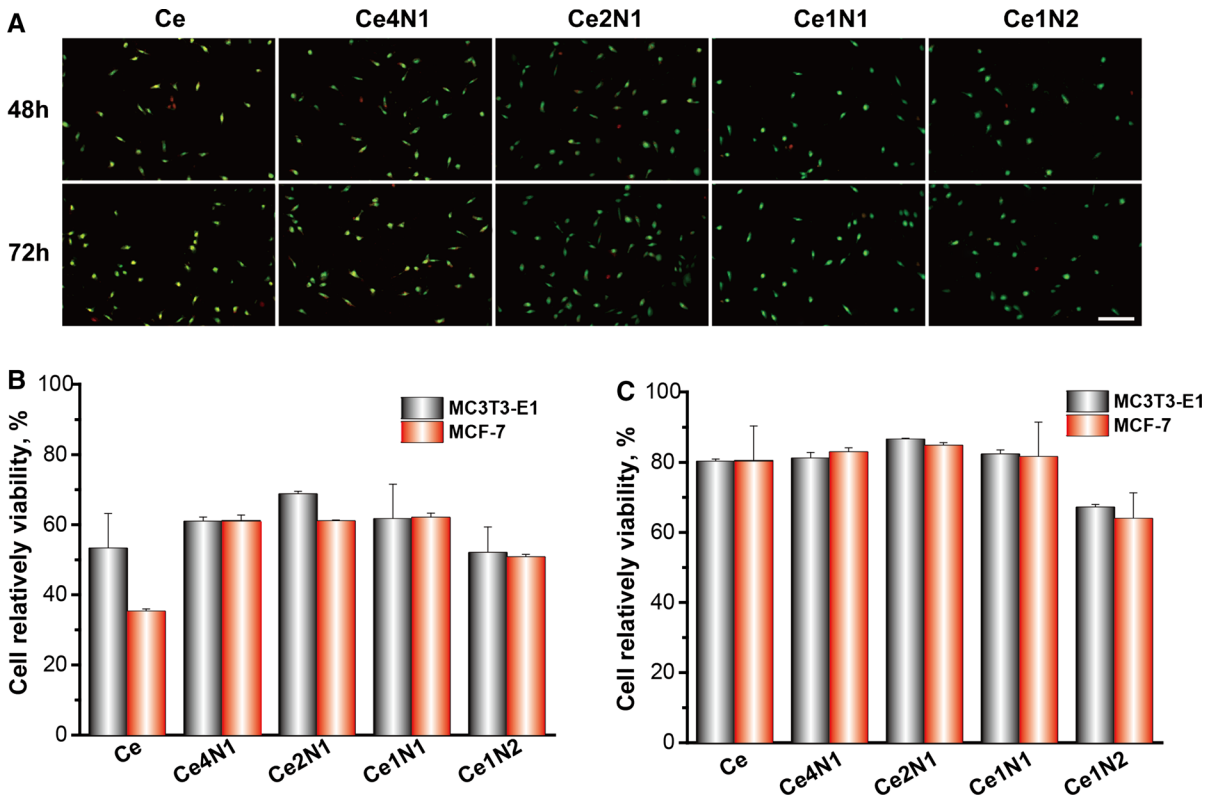

Fig. 8 **a** Fluorescent images of MC3T3-E1 cells on the Ce and cellulose/HNT composite hydrogels, *Scale bar* 100 μm. The MC3T3-E1 and MCF-7 cells viability of the hydrogels determined by CCK-8 at 48 h (**b**) and 72 h (**c**)

with the pure cellulose hydrogel (except the Ce1N2). Cells can proliferate with the increased incubation time, demonstrating that the hydrogels have unbiased biocompatibility. After 72 h, the composite hydrogels show comparable cell viability with the pure cellulose hydrogel. The relative viability of cells growth on the Ce1N2 hydrogel surface is slightly lower than that of other samples, which is probably due to the inhibition effect on cell growth of excessive HNT in the hydrogels (66.7 wt%)(Vergaro et al. 2010).

Drug-loading and release studies and cytotoxicity of curcumin incorporated hydrogels

To evaluate the potential of the cellulose/HNT composite hydrogel applied in biomaterials, the drug-loading properties and cytotoxicity of the curcumin-loaded hydrogels were assessed. The Ce and Ce1N1 hydrogels were placed in curcumin ethanol solution to adsorption equilibrium. Figure 9a compares the loading capacity and entrapment efficiency of Ce and Ce1N1 hydrogel. It can be seen that the two hydrogels show nearly same loading capacity of 4.1% for curcumin. However, the entrapment efficiency of curcumin of the Ce1N1 hydrogel (21%) is well above that of Ce hydrogel (17%). This should be attributed to the synergistic effects of HNT with cellulose in the composite hydrogels, as both the raw HNT and cellulose have high adsorption ability for active molecules (Luo et al. 2010; Wojnárovits et al. 2010). The drug release behavior of curcumin-loaded hydrogels is shown in Fig. 9b. From the inset in Fig. 9b, both the hydrogels can be uniformly stained with yellow color by the loaded curcumin. Both Ce and Ce1N1 hydrogels show a controlled release behavior of curcumin up to 20 h, which suggests the hydrogels can be a good carrier for drug delivery. Compared with pure cellulose hydrogel, the drug in the Ce1N1 hydrogel is released with a much slower rate. The curcumin is not uniformly released from the Ce hydrogel, and the release is almost completed after 12 h. In contrast, Ce1N1 exhibits a relatively slow

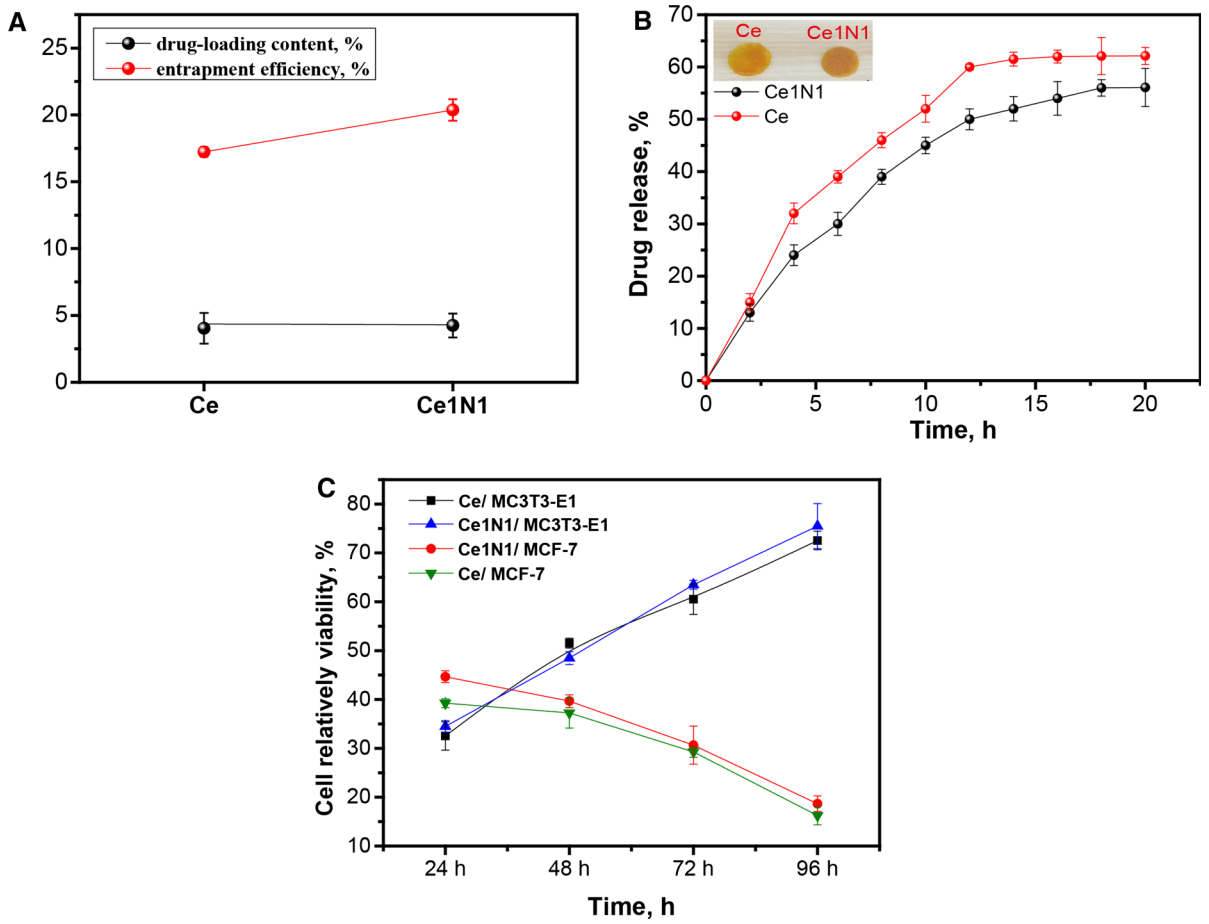

Fig. 9 **a** Drug loading capacity and entrapment efficiency of Ce and Ce1N1 hydrogels. **b** The drug-release curves of curcumin-loaded Ce and Ce1N1 hydrogels in pure ethanol solution (*inset* shows the appearance of the drug-loaded hydrogels). **c** The MC3T3-E1 and MCF-7 cell viability of the curcumin-loaded hydrogels determined by CCK-8

release behavior towards curcumin, which indicates that the increased drug-materials interactions in the composite hydrogels. HNTs exhibit a tubular structure with large specific surface areas, so they have strong drug adsorption properties. The loaded drug can slowly escape from the tubular structures of HNT due to a steric hindrance effect, which is extensively used as a drug carrier (Levis and Deasy 2002; Lvov et al. 2008). Therefore, the incorporation of HNT can improve the drug-loading capacity and sustained-release effect of cellulose hydrogel. The final drug release ratio for Ce and Ce1N1 hydrogel after 20 h is 56.1 and 62.1%, respectively. Curcumin is believed to have anti-inflammatory, antioxidant, and even anti-cancer properties (Divakaran et al. 2016; Jiang et al. 1996; Mukhopadhyay et al. 2001; Ravindran et al. 2009). So, the cell viability of the curcumin-loaded hydrogel was further evaluated by the CCK-8 method, and the results are presented in Fig. 9c. Interestingly, the MC3T3-E1 cells show a high relative activity and proliferation ability for the curcumin-loaded hydrogels, while the MCF-7 cells appear to have a trend of apoptosis with the increase of incubation time. Besides, the relative activity of MCF-7 cells cultured on Ce1N1 hydrogel is slightly higher than that of cell growth on Ce hydrogel, which is related to the release rate of curcumin loaded on the Ce hydrogel is faster than that of Ce1N1.

Figure 10 further demonstrates fluorescent images of MC3T3-E1 and MCF-7 cells treated by curcumin-loaded hydrogels. In the control group, the cells grow and proliferate well but with different shape (MCF-7 cells grow in an inverted triangle shape and MC3T3-E1 cells grow in an oval shape). The MC3T3-E1 cell

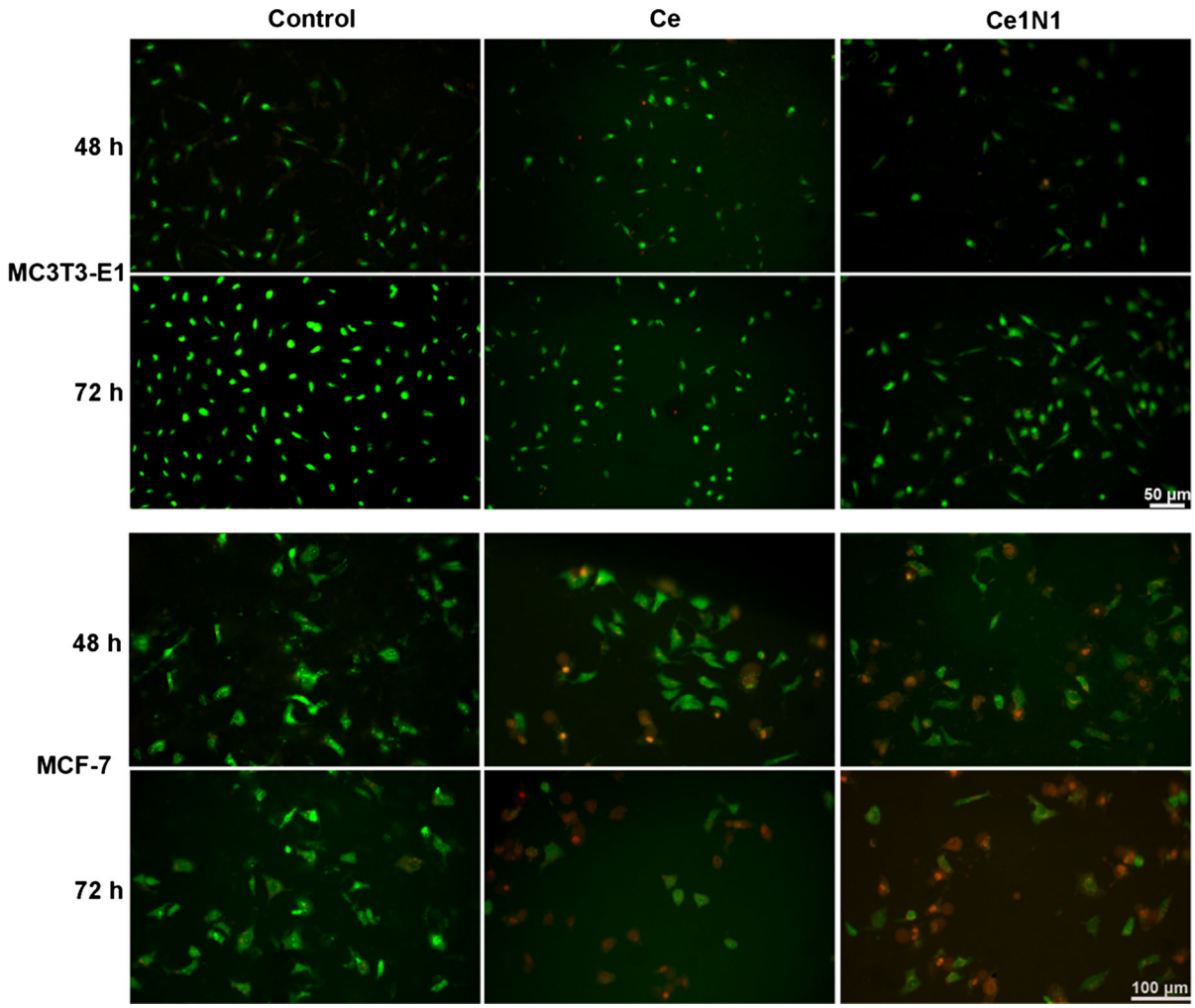

Fig. 10 Fluorescent images of MC3T3-E1 and MCF-7 cells cultured on the curcumin-loaded hydrogels

growth on the curcumin-loaded hydrogel is almost no different from that on the control group, illustrating that the loading of curcumin has no effect on the growth of the normal cells. In contrast, the red color in the MCF-7 cells increases markedly with the increase of incubation time from 48 to 72 h, indicating MCF-7 cells present the characteristic morphology of apoptosis. This morphology results are highly consistent with the CCK-8 results above. In short, the cytotoxicity experiments demonstrate that the curcumin-loaded hydrogels have a slight effect on the normal cells while showing inhibition effects for tumor cells growth. These hydrogels provide a possible application as an anticancer drug delivery system and as an anti-inflammatory wound dressing.

Conclusions

HNTs are incorporated into cellulose NaOH/urea solution to prepare composite hydrogels using epichlorhydrine crosslinking at elevated temperature. The viscosity of the composite solution increases with the addition of HNT. The compressive mechanical properties and resistance to deformation properties of composite hydrogels significantly increase compared to pure cellulose hydrogels. XRD and FTIR show that the crystal structure and chemical structure of HNT are not changed in the composite hydrogels. Hydrogen bonding interactions between HNT and cellulose exist in the composites. The addition of HNT leads to decreased pore size and decreased swelling ratios in NaCl solution and pure water. Both of the normal cell

and the tumor cells show a high cell relative viability on composites hydrogels. Curcumin can be successfully loaded into the hydrogels via physical adsorption. The curcumin-loaded composite hydrogels show a strong inhibition effect on the MCF-7 cells while showing good cytocompatibility for MC3T3-E1 cells. All the results illustrate that the cellulose/HNT composite hydrogels have promising applications such as anticancer drug delivery systems and anti-inflammatory wound dressings.

Acknowledgements This work was financially supported by the National High Technology Research and Development Program of China (2015AA020915), the National Natural Science Foundation of China (51473069 and 51502113), and the Guangdong Natural Science Funds for Distinguished Young Scholar (S2013050014606), Science and Technology Planning Project of Guangdong Province (2014A020217006), Guangdong Special Support Program (2014TQ01C127), the Special Fund for Ocean-Scientific Research in the public interest (201405105), and the Pearl River S&T Nova Program of Guangzhou (201610010026).

References

Abdullayev E, Joshi A, Wei W et al (2012) Enlargement of halloysite clay nanotube lumen by selective etching of aluminum oxide. ACS Nano 6(8):7216–7226

Ariga K, Lvov YM, Kawakami K et al (2011) Layer-by-layer self-assembled shells for drug delivery. Adv Drug Deliv Rev 63(9):762–771

Cai J, Zhang L (2005) Rapid dissolution of cellulose in LiOH/urea and NaOH/urea aqueous solutions. Macromol Biosci 5(6):539–548

Cai J, Liu S, Feng J et al (2012) Cellulose–silica nanocomposite aerogels by in situ formation of silica in cellulose gel. Angew Chem 124(9):2118–2121

Cavallaro G, Lazzara G, Konnova S et al (2014) Composite films of natural clay nanotubes with cellulose and chitosan. Green Mater 2(4):232

Ciolacu D, Ciolacu F, Popa VI (2011) Amorphous cellulose—structure and characterization. Cellul Chem Technol 45(1):13

De Oliveira Barud HG, Da Silva RR, Da Silva Barud H et al (2016) A multipurpose natural and renewable polymer in medical applications: bacterial cellulose. Carbohydr Polym 153:406–420

Demilecamps A, Reichenauer G, Rigacci A et al (2014) Cellulose–silica composite aerogels from "one-pot" synthesis. Cellulose 21(4):2625–2636

Divakaran AV, Azad LB, Surwase SS et al (2016) Mechanically tunable curcumin incorporated polyurethane hydrogels as potential biomaterials. Chem Mater 28(7):2120–2130

Eichhorn SJ, Dufresne A, Aranguren M et al (2010) Review: current international research into cellulose nanofibres and nanocomposites. J Mater Sci 45(1):1–33

French AD (2014) Idealized powder diffraction patterns for cellulose polymorphs. Cellulose 21(2):885–896

Hanid NA, Wahit MU, Guo Q et al (2014) Development of regenerated cellulose/halloysites nanocomposites via ionic liquids. Carbohydr Polym 99:91–97

Huang B, Liu M, Long Z et al (2017) Effects of halloysite nanotubes on physical properties and cytocompatibility of alginate composite hydrogels. Mater Sci Eng, C 70:303–310

Jiang MC, Yang-Yen HF, Yen JJY et al (1996) Curcumin induces apoptosis in immortalized NIH 3T3 and malignant cancer cell lines. Nutr Cancer 26(1):111–120

Klemm D, Heublein B, Fink HP et al (2005) Cellulose: fascinating biopolymer and sustainable raw material. Angew Chem Int Ed 44(22):3358–3393

Levis S, Deasy P (2002) Characterisation of halloysite for use as a microtubular drug delivery system. Int J Pharm 243(1):125–134

Li S-M, Jia N, Ma M-G et al (2011) Cellulose–silver nanocomposites: microwave-assisted synthesis, characterization, their thermal stability, and antimicrobial property. Carbohydr Polym 86(2):441–447

Liu M, Guo B, Du M et al (2007) Properties of halloysite nanotube–epoxy resin hybrids and the interfacial reactions in the systems. Nanotechnology 18(45):455703

Liu M, Li W, Rong J et al (2012) Novel polymer nanocomposite hydrogel with natural clay nanotubes. Colloid Polym Sci 290(10):895–905

Liu M, Wu C, Jiao Y et al (2013a) Chitosan–halloysite nanotubes nanocomposite scaffolds for tissue engineering. J Mater Chem B 1(15):2078–2089

Liu M, Zhang Y, Li J et al (2013b) Chitin-natural clay nanotubes hybrid hydrogel. Int J Biol Macromol 58:23–30

Liu M, Jia Z, Jia D et al (2014a) Recent advance in research on halloysite nanotubes-polymer nanocomposite. Prog Polym Sci 39(8):1498–1525

Liu M, Shen Y, Ao P et al (2014b) The improvement of hemostatic and wound healing property of chitosan by halloysite nanotubes. RSC Adv 4(45):23540–23553

Liu M, Huang J, Luo B et al (2015) Tough and highly stretchable polyacrylamide nanocomposite hydrogels with chitin nanocrystals. Int J Biol Macromol 78:23–31

Liu M, Chang Y, Yang J et al (2016a) Functionalized halloysite nanotube by chitosan grafting for drug delivery of curcumin to achieve enhanced anticancer efficacy. J Mater Chem B 4(13):2253–2263

Liu M, He R, Yang J et al (2016b) Polysaccharide–halloysite nanotube composites for biomedical applications: a review. Clay Miner 51(3):457–467

Liu M, He R, Yang J et al (2016c) Stripe-like clay nanotubes patterns in glass capillary tubes for capture of tumor cells. ACS Appl Mater Interfaces 8(12):7709–7719

Luo P, Zhao Y, Zhang B et al (2010) Study on the adsorption of Neutral Red from aqueous solution onto halloysite nanotubes. Water Res 44(5):1489–1497

Lvov YM, Shchukin DG, Mohwald H et al (2008) Halloysite clay nanotubes for controlled release of protective agents. ACS Nano 2(5):814–820

Lvov Y, Wang W, Zhang L et al (2016) Halloysite clay nanotubes for loading and sustained release of functional compounds. Adv Mater 28(6):1227–1250

Maneerung T, Tokura S, Rujiravanit R (2008) Impregnation of silver nanoparticles into bacterial cellulose for antimicrobial wound dressing. Carbohydr Polym 72(1):43–51

Meibom KL, Li XB, Nielsen AT et al (2004) The *Vibrio cholerae* chitin utilization program. Proc Natl Acad Sci USA 101(8):2524–2529

Miao C, Hamad WY (2013) Cellulose reinforced polymer composites and nanocomposites: a critical review. Cellulose 20(5):2221–2262

Mukhopadhyay A, Bueso-Ramos C, Chatterjee D et al (2001) Curcumin downregulates cell survival mechanisms in human prostate cancer cell lines. Oncogene 20(52):7597–7609

Pandey G, Munguambe DM, Tharmavaram M et al (2017) Halloysite nanotubes-An efficient 'nano-support'for the immobilization of α-amylase. Appl Clay Sci 136:184–191

Price RR, Gaber BP, Lvov Y (2001) In-vitro release characteristics of tetracycline HCl, khellin and nicotinamide adenine dineculeotide from halloysite; a cylindrical mineral. J Microencapsul 18(6):713–722

Ravindran J, Prasad S, Aggarwal BB (2009) Curcumin and cancer cells: how many ways can curry kill tumor cells selectively? AAPS J 11(3):495–510

Ren X, Chen D, Meng X et al (2009) Amperometric glucose biosensor based on a gold nanorods/cellulose acetate composite film as immobilization matrix. Colloids Surf B 72(2):188–192

Russo R, Malinconico M, Santagata G (2007) Effect of cross-linking with calcium ions on the physical properties of alginate films. Biomacromol 8(10):3193–3197

Soheilmoghaddam M, Wahit MU, Mahmoudian S et al (2013) Regenerated cellulose/halloysite nanotube nanocomposite films prepared with an ionic liquid. Mater Chem Phys 141(2):936–943

Suzuki M, Hanabusa K (2010) Polymer organogelators that make supramolecular organogels through physical cross-linking and self-assembly. Chem Soc Rev 39(2):455–463

Vergaro V, Abdullayev E, Lvov YM et al (2010) Cytocompatibility and uptake of halloysite clay nanotubes. Biomacromol 11(3):820–826

Wan C, Jiao Y, Li J (2017) Flexible, highly conductive, and free-standing reduced graphene oxide/polypyrrole/cellulose hybrid papers for supercapacitor electrodes. J Mater Chem A. doi:10.1039/C6TA04844G

Wojnárovits L, Földváry CM, Takács E (2010) Radiation-induced grafting of cellulose for adsorption of hazardous water pollutants: a review. Radiat Phys Chem 79(8): 848–862

Yang J, Wu Y, Shen Y et al (2016) Enhanced therapeutic efficacy of doxorubicin for breast cancer using chitosan oligosaccharide-modified halloysite nanotubes. ACS Appl Mater Interfaces 8(40):26578–26590

Yu X, Tong S, Ge M et al (2013) Removal of fluoride from drinking water by cellulose@ hydroxyapatite nanocomposites. Carbohydr Polym 92(1):269–275

Yuan P, Southon PD, Liu Z et al (2008) Functionalization of halloysite clay nanotubes by grafting with γ-aminopropyltriethoxysilane. J Phys Chem C 112(40):15742–15751

Zhang H, Wang Z, Zhang Z et al (2007) Regenerated-cellulose/multiwalled-carbon-nanotube composite fibers with enhanced mechanical properties prepared with the ionic liquid 1-allyl-3-methylimidazolium chloride. Adv Mater 19(5):698–704

Zhang X, Liu X, Zheng W et al (2012) Regenerated cellulose/graphene nanocomposite films prepared in DMAC/LiCl solution. Carbohydr Polym 88(1):26–30

Zhu B-K, Xie S-H, Xu Z-K et al (2006) Preparation and properties of the polyimide/multi-walled carbon nanotubes (MWNTs) nanocomposites. Compos Sci Technol 66(3):548–554